Global and Planetary Change 249 (2025) 104791

Contents lists available at ScienceDirect

Global and Planetary Change

journal homepage: www.elsevier.com/locate/gloplacha

Research Article

Exploring Neoproterozoic climate and biogeochemical evolution in the SCION model

Benjamin J.W. Mills [a,*], Guillaume le Hir [b], Andrew Merdith [c], Khushboo Gurung [a], Fred T. Bowyer [a], Alexander J. Krause [a,d], Patricia Sanchez-Baracaldo [e], Stephen J. Hunter [a], Yinggang Zhang [f]

[a] School of Earth and Environment, University of Leeds, Leeds LS2 9JT, UK
[b] Université Paris, Institut de Physique du Globe de Paris, CNRS, 1 rue Jussieu, 75005 Paris, France
[c] School of Physics, Chemistry and Earth Sciences, University of Adelaide, Adelaide, Australia
[d] School of Earth and Environmental Sciences, Cardiff University, Main Building, Cardiff CF10 3AT, UK
[e] School of Geographical Sciences, University of Bristol, Bristol, UK
[f] Nanjing Institute of Geology and Palaeontology, Chinese Academy of Sciences, Nanjing, China

ARTICLE INFO

Editor: Dr. Maoyan Zhu

Keywords:
Carbon cycle
Biogeochemistry
Deep time
Precambrian
Climate
Modeling

ABSTRACT

The Neoproterozoic Era (1000–539 Ma) saw extreme changes in climate and biogeochemical cycles, but the drivers of these changes remain poorly understood. In this paper, we extend the Spatial Continuous Integration (SCION) global climate-biogeochemical model beyond the Phanerozoic and into the Neoproterozoic using a set of GCM simulations to update the model's climate emulator and a plate tectonic model to estimate tectonic input fluxes. We use the model to explore to what degree changes in paleogeography and degassing rates—which are key drivers of Phanerozoic climate—can explain the broad pattern of Neoproterozoic environmental change. We find that while the known Neoproterozoic climate changes are generally within the model uncertainty envelope, and the model predicts cooling between the later Tonian and Earliest Cryogenian, we do not reproduce a clear greenhouse to icehouse transition here, or any long-term increases in atmospheric oxygen levels before the Ediacaran. Several key model limitations currently prevent it from testing these ideas in more detail and should be improved in future work. These include: dynamic continental lithology, climate simulations which include dynamic continental ice sheets, a more comprehensive estimate of degassing rates, a better representation of the evolution of primary producer groups (i.e. planktonic cyanobacteria and green algae) and the spatial structure of marine biogeochemistry, and a dynamic calcium cycle. We anticipate that these can all be tested in the future within the SCION framework.

1. Climate and biogeochemistry of the Neoproterozoic Era

The Neoproterozoic Era is almost as long as the entire Phanerozoic Eon, lasting from 1000 Ma to ≤538.8 Ma (≥533 Ma). It directly precedes the Phanerozoic and is generally thought to have been a time of rising oxygen levels in both the atmosphere and oceans (Canfield et al., 2007; Krause et al., 2022; Stockey et al., 2024), which coincided with the evolution of the first animals towards the end of the Era in the Ediacaran Period (e.g. Dunn et al., 2022). In this way, the Neoproterozoic appears to document a transition from the oxygen-poor environments and microbial ecosystems of the Proterozoic towards the oxygenated and animal-supporting ecosystems of the Phanerozoic. The Neoproterozoic also saw a dramatic long-term perturbation in Earth's climate, from a greenhouse climate state during the Tonian Period to a severe period of icehouse climates during the Cryogenian (Hoffman et al., 1998). The degree of cooling, and persistence and spatial extent of ice cover during the two Cryogenian 'Snowball Earth' glaciations remains uncertain (e.g. Song et al., 2023), but conditions were undoubtedly colder than at any point during the Phanerozoic.

Several hypotheses have been developed to explain the occurrence of Neoproterozoic oxygenation and extreme glaciation. Amongst them is the idea that long-term oxygenation may ultimately stem from increases in the transfer of carbon from the lithosphere to the atmosphere through degassing, which results in greater rates of photosynthesis (Williams

* Corresponding author.
E-mail address: B.Mills@leeds.ac.uk (B.J.W. Mills).

https://doi.org/10.1016/j.gloplacha.2025.104791
Received 3 October 2024; Received in revised form 29 January 2025; Accepted 9 March 2025
Available online 13 March 2025

et al., 2019; Alcott et al., 2024). Alternatively, cooling may be caused by a decrease in these same tectonic carbon inputs, which result in a restricted supply of atmospheric CO_2 (Dutkiewicz et al., 2024; Mills et al., 2017). Another line of investigation concerns changes to paleogeography—particularly the Neoproterozoic breakup of the supercontinent Rodinia—which may have increased global runoff rates and could have led to enhanced silicate weathering and thus cooling (Donnadieu et al., 2004). This could also have increased the supply of the limiting nutrient, phosphate, to drive photosynthesis and oxygenation.

These hypotheses about changes in degassing rates, paleogeography and primary production mirror key hypotheses for Phanerozoic Earth system change—where changes to degassing and paleogeography, and their effects on productivity, are thought to be major factors controlling long-term global temperature and oxygen levels (Goddéris et al., 2023; Mills et al., 2021; Lenton et al., 2018). However, while testing these ideas in the Phanerozoic has been possible through detailed biogeochemical models and comparisons to geochemical datasets, they have remained largely untested for the Neoproterozoic. Thus, in this paper we extend the SCION global climate-biogeochemical model for Phanerozoic time into the Neoproterozoic to better understand whether 'Phanerozoic-style' climate and biogeochemical drivers can be responsible for Neoproterozoic Earth system change. This is not to say that paleogeography and degassing rate changes can explain all of Phanerozoic climate, but many other proposed climate and redox state modifiers such as Large Igneous Provinces (LIPs, e.g. Black et al., 2024) have not yet been consistently integrated over Phanerozoic time.

2. Phanerozoic biogeochemical models and SCION

Since the first GEOCARB model (Berner, 1991), several numerical models have attempted to reconstruct long-term Phanerozoic biogeochemistry (e.g. GEOCARBSULF: Royer et al., 2014; MAGic: Arvidson et al., 2013; COPSE: Lenton et al., 2018). These models aim to track the movement of carbon and other important elements through nondimensional reservoirs ('boxes') which represent the Earth's atmosphere, oceans and crust over multimillion year timescales. They can make predictions about past atmospheric and oceanic compositions where data are unavailable, or in cases where reliable data are available, these models can test what processes control the Earth's surface chemistry and climate state.

While the structure of these 'box models' is simple, they are still powerful tools. They dynamically simulate many separate elemental cycles and their interactions with each other, and they produce these simulations continuously over very long time periods where they can be tested against large independent databases of geological data. This means that there are many routes to model falsification, which makes the models useful for hypothesis testing. Phanerozoic-scale continuous biogeochemical models (i.e. running over the whole Phanerozoic) have been used to test the processes driving cooling during the late Ordovician (Lenton et al., 2012; Longman et al., 2021), the Permo-Carboniferous (Bergman et al., 2004; Berner, 1997) and the Cenozoic (Brune et al., 2017; Van Der Meer et al., 2014). They have also been used to test the hypothesis that early Paleozoic oxygen levels were lower than present (Lenton et al., 2016; Krause et al., 2018), and that Permo-Carboniferous oxygen levels were higher (Berner, 2006; Bergman et al., 2004) and they have been used to reconstruct marine sulfate levels over Phanerozoic time and investigate the processes which control sulfate availability (Lenton et al., 2018; Krause et al., 2024).

Building on these approaches, a more recent model, SCION (Mills et al., 2021; Fig. 1), is currently the most comprehensive continuous Phanerozoic-scale global biogeochemical model. It extends the established box model approaches by adding a 3D climate emulator (based on GEOCLIM; Goddéris et al., 2014) and a 2D continental weathering scheme (based on West, 2012 and Maffre et al., 2018) to the biogeochemical box model system from COPSE (Tostevin and Mills, 2020). SCION is therefore able to represent processes like continental weathering and terrestrial productivity in a much more realistic way than the other box models (e.g. Gurung et al., 2022, 2024), while still retaining the ability to run continuously over Phanerozoic time.

Like the GEOCARBSULF and COPSE models, SCION principally computes the long-term carbon, oxygen and sulfur cycles. To do this it calculates the fluxes of weathering, burial and metamorphism/degassing which move compounds between the hydrosphere (a combined ocean-atmosphere box) and crust. For both the carbon and sulfur cycles,

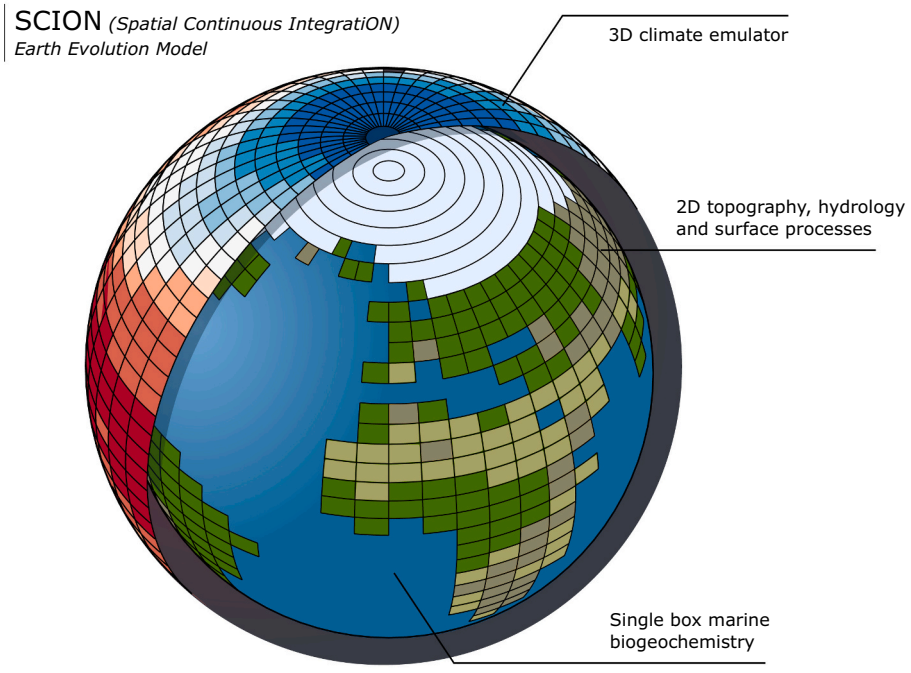

Fig. 1. SCION model overview. A 3D climate emulator is linked dynamically to a 2D surface scheme and single box atmosphere-ocean-sediment biogeochemical scheme.

the burial of reduced species (organic carbon and pyrite respectively) oxygenates the surface system, whereas their weathering or degassing consumes oxygen. Following COPSE, SCION includes dynamic marine phosphate and nitrate reservoirs, and uses the concentration of these limiting nutrients to calculate the rate of new production and carbon burial. It also calculates isotopic ratios of carbon, sulfur and strontium which can be compared directly to the geological record.

The spatially-resolved climate and surface processes in SCION allow it to represent the paleogeographic enhancement of weathering. For example, microcontinents in humid latitudes are subject to intense weathering, whereas continental interiors (especially in the drier subtropics) tend to be arid and have more restricted weathering (e.g. Goddéris et al., 2014, 2023). The model also represents the topographical enhancement of weathering, where mountain belts drive orographic uplift, rainfall and erosion, which can contribute to rapid chemical weathering in these areas (Maher and Chamberlain, 2014). Silicate weathering is a key long-term sink of atmospheric CO_2—both directly through delivery of alkalinity and subsequent precipitation of carbonates, and indirectly through the delivery of nutrients like phosphate to the oceans, which drives organic carbon burial (Witkowski et al., 2018). The spatially-resolved representation of silicate weathering means that SCION is able to produce a long cooling interval roughly coincident with the Late Paleozoic Ice Age (LPIA, ~360–260 Ma), which is driven in the model by the uplift of the low latitude Hercynian mountain belt (Goddéris et al., 2017a, 2017b; Mills et al., 2021). It also produces a high-CO_2 Triassic period, broadly consistent with geological data, due in part to the aridity of Pangaea during this time which restricted weathering and CO_2 removal (Mills et al., 2021), as well as limiting the geographic range of plants (Gurung et al., 2024).

SCION also makes reasonably consistent predictions for atmospheric oxygen concentrations over the Phanerozoic. A key feature of the geological reconstruction of Phanerozoic O_2 is an apparent rise in oxygen levels between the Ordovician and Devonian periods (Dahl et al., 2010; Sperling et al., 2015; Mills et al., 2023). This is reproduced in SCION through the assumption that land plants expanded at this time, and in doing so they increased the rates of terrestrial-derived organic carbon burial—as was previously explored in the COPSE model (Bergman et al., 2004; Lenton et al., 2016). A further rise in O_2 levels to >30 % of the atmosphere during the Carboniferous-Permian is a feature of several proxy-derived interpretations (Berner and Canfield, 1989; Algeo and Ingall, 2007; Berner, 2009), but is not currently reproduced by SCION. The model also fails to reproduce low marine sulfate in the Cambrian to Carboniferous periods which has been inferred from the generally low fractionation between pyrite and sulfate from these times, alongside fluid inclusion data (Algeo et al., 2015). It is likely that this is at least partly because the model does not have a dynamic calcium cycle (Krause et al., 2024).

Overall, neither the box models or the 3D approaches in SCION and GEOCLIM have convincingly replicated the whole timeline of Phanerozoic biogeochemistry and climate. Efforts are underway to further investigate the mismatches noted above and to increase model complexity, and the process of extending the model timeframe in this paper is part of that effort. By exploring new timeframes and events it may be possible to make a discovery that improves our understanding for other time periods. We now discuss our extension of the model timeframe, but return to further discuss model limitations and possible improvements for both the Neoproterozoic and Phanerozoic at the end of the paper.

3. Extending SCION into the Neoproterozoic

We begin this work with model version 1.1.6, which can be accessed freely using the repository link at the end of the manuscript. To extend the model to cover Neoproterozoic time, we first update the climate emulator with Neoproterozoic runs of the FOAM climate model (Jacob, 1997). We use a previously computed set of model runs for six paleogeographical configurations between 825 Ma and 580 Ma (Goddéris et al., 2017b), where the paleogeography is taken from Li et al. (2013). The topography and shallow marine bathymetry here follow the facies analysis of Li et al. (2013), considering geological constraints to classify orogens by age and deriving elevation estimates from Cenozoic analogues for young orogens and through denudation estimates for old orogens. To avoid unrealistically flat regions over large areas, these maps include a noise function for regions outside of elevated terrain. Shallow shelf depths are informed by Phanerozoic examples, and deep marine bathymetry is fixed at a ~ 4 km depth. These climate model runs were performed at a range of CO_2 concentrations between 3× and 48× preindustrial, allowing the emulator in SCION to dynamically prescribe climate fields as the model time and CO_2 level changes (see Mills et al., 2021 for a schematic and description of the emulator).

We next update the global tectonic degassing rate in the model, which is used as a scaling for all metamorphic and degassing processes (Fig. 2). The Phanerozoic SCION model used an uncertainty window for degassing rates to incorporate different estimation methods. The overall window was bounded by estimates of overall plate convergence and destruction rates (Domeier and Torsvik, 2017; Marcilly et al., 2021) as the upper estimate, and combined lengths of subduction zones and rifts as the lower estimate (Mills et al., 2017, 2019). For the Neoproterozoic extension we first add the estimates of Krause et al. (2022), who defined upper estimates as the mantle-to-crust plate fluxes or rift lengths, and lower estimates as the subduction zone lengths, with these datasets extracted from the plate model of Merdith et al. (2021). We then also add the alternative estimate of Marcilly et al. (2021) who scale the global degassing rate over Earth history to the age-distribution frequency of detrital zircons, reasoning that zircon age distributions are closely related to magmatic productivity (Domeier et al., 2018). The combined Phanerozoic and Neoproterozoic windows from previous work show reasonable agreement with the zircon-based estimate, and thus we combine all three to define a grouped minimum and maximum for this study (Fig. 2b).

Finally, we modify the model 'basalt area' and 'granite area' forcings to best represent how they may have been different during the Neoproterozoic (Fig. 2c). These functions affect the isotopic ratio of weathered strontium in the model, so only impact the $^{87}Sr/^{86}Sr$ record the model produces, with no effect on climate or biogeochemistry. For basalt area, we retain the original model approach, which uses the database of reconstructed initial areas of Large Igneous Provinces (LIPs) alongside a decay curve to estimate total continental flood basalt area (Ernst and Youbi, 2017; Mills et al., 2014), and add a further term for arc weathering, scaled to global volcanism (Mills et al., 2019). For granite area, we retain the original curve, derived from geological maps of non-volcanic silicates (Bluth and Kump, 1991; Lenton et al., 2018) and make the simplifying assumption that the value begins at the present-day area in the Tonian and slowly interpolates towards the Cambrian value. The evolutionary model forcings, which control the spread of plants and marine bioturbators, do not need to be extended into the Neoproterozoic, as they only become significant during Phanerozoic time. We also omit the FLORA vegetation model from this version of SCION, as it has not yet been fully integrated before the Mesozoic (Gurung et al., 2024).

3.1. Results and comparisons

The key biogeochemical model outputs are shown in Fig. 3. Here, the yellow window represents the full range of outputs generated over 1000 model runs when randomly varying the model forcings for degassing rate, pre-plant weathering enhancement, basalt and granite areas, and fractionation effects for carbon and sulfur isotopes. The ranges of variation are described in Mills et al. (2021) and are typically ±20–30 %, except for the pre-plant weathering value which varies between 1 (no change) and a seven-fold enhancement, and the degassing rate which varies between the maximum and minimum values shown in Fig. 2.

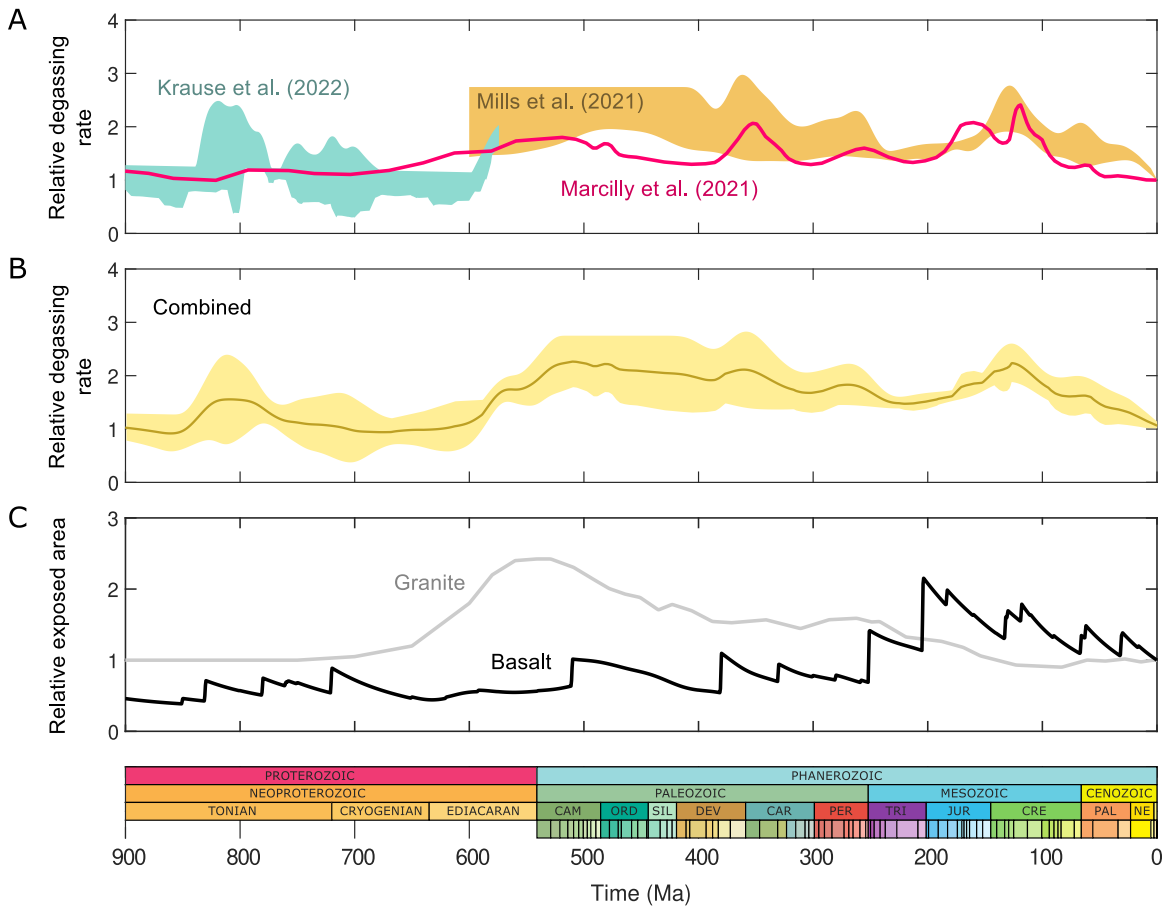

Fig. 2. Model degassing rates and weatherable areas. A. Degassing rates from previous studies. B. Combined degassing rate used for the current model. Note that smoothing has been applied to remove rapid transitions in the Neoproterozoic record, which are uncertain, and to make the overall variability of the combined record consistent, despite the merging of different approaches. C. Weatherable areas of granite and basalt.

These large degrees of variation explain the wide uncertainty window for model results in the Neoproterozoic and Paleozoic. Here, the degassing rate is less certain, due to underlying uncertainty in plate reconstruction for pre-Pangaea times, and the reduction in continental weathering efficiency due to the absence of forests before the Devonian, and absence of all plants before the Ordovician, is not well quantified (Lenton, 2001).

The trend for Neoproterozoic oxygen, sulfate and carbon dioxide levels is similar, with all concentrations rising slightly across the early-mid Tonian and declining into the Cryogenian. This behaviour follows the model degassing rate: CO_2 degassing is a first-order control on atmospheric CO_2 levels, and high rates of carbon input will ultimately lead to high rates of carbon output—including organic carbon burial—which raises atmospheric oxygen in line with CO_2 (e.g. Williams et al., 2019). Warmer climates and higher oxygen levels favour weathering inputs of sulfate from evaporites and pyrite, so marine sulfate levels also tend to track CO_2 and O_2. This coupled behaviour continues until the Devonian in the model, where the evolution of plants—which produce O_2 but draw down CO_2 through photosynthesis and enhancement of silicate weathering—changes the global relationship between CO_2 and O_2.

The model is compared to previous estimates from geological proxy and model systems which are plotted in blue (see Fig. 3 and caption). Some of these estimates also have large uncertainty windows, and tend to be broadly defined such that an invariant upper or lower boundary does not necessarily mean that values did not fluctuate considerably within these limits. Considering this high uncertainty, the predicted CO_2 and global average temperature values are broadly compatible with previous estimates. CO_2 levels in SCION overlap with those from previous dimensionless numerical modeling (Krissansen-Totton et al., 2018). The mean global average temperature predicted by the model for the Neoproterozoic is around 15–20 °C, similar to many periods of the Phanerozoic and representing a mild icehouse to mild greenhouse climate state with ice caps restricted to the polar regions. However, within the model uncertainty window, it is possible to reach global average temperatures of between approximately 0–30 °C and to see deep glaciation on par with the coldest times in the Phanerozoic. We do not create 'Snowball Earth' globally ice-covered scenarios in the model. Partly this is because we likely do not see cold enough surface temperatures (Le Hir et al., 2014), and also because the climate model used to build the emulator does not have dynamic continental ice sheets, so cannot simulate the descent into a 'Snowball Earth' state through ice-albedo feedback (e.g. Hoffman and Schrag, 2002; Hoffman et al., 2017).

Model atmospheric O_2 predictions are compatible with some proxy inferences which suggest that the Neoproterozoic atmospheric oxygen level was around half or less of the Present Atmospheric Level (PAL: 0.5 PAL = ~10 % atm.) (Mills et al., 2023), based on requirements of broadly anoxic marine bottom waters (e.g. Sperling et al., 2015; Canfield, 1998). However, recent analyses of trace metal abundances in sediments suggest an upper limit of only around 0.1 PAL or 2 % atm (Stockey et al., 2024). Inversion of Neoproterozoic carbon isotope records suggests large swings in carbon burial and atmospheric O_2 during the Era, with potential minimums of 0.01–0.1 PAL (~ < 2 % atm.; Krause et al., 2022). These lower values, or large swings, are not reproduced by SCION and are not within the uncertainty window, but they could feasibly be driven by other events not included in the model such as 'Snowball Earth' glaciations, or by more rapid variations in

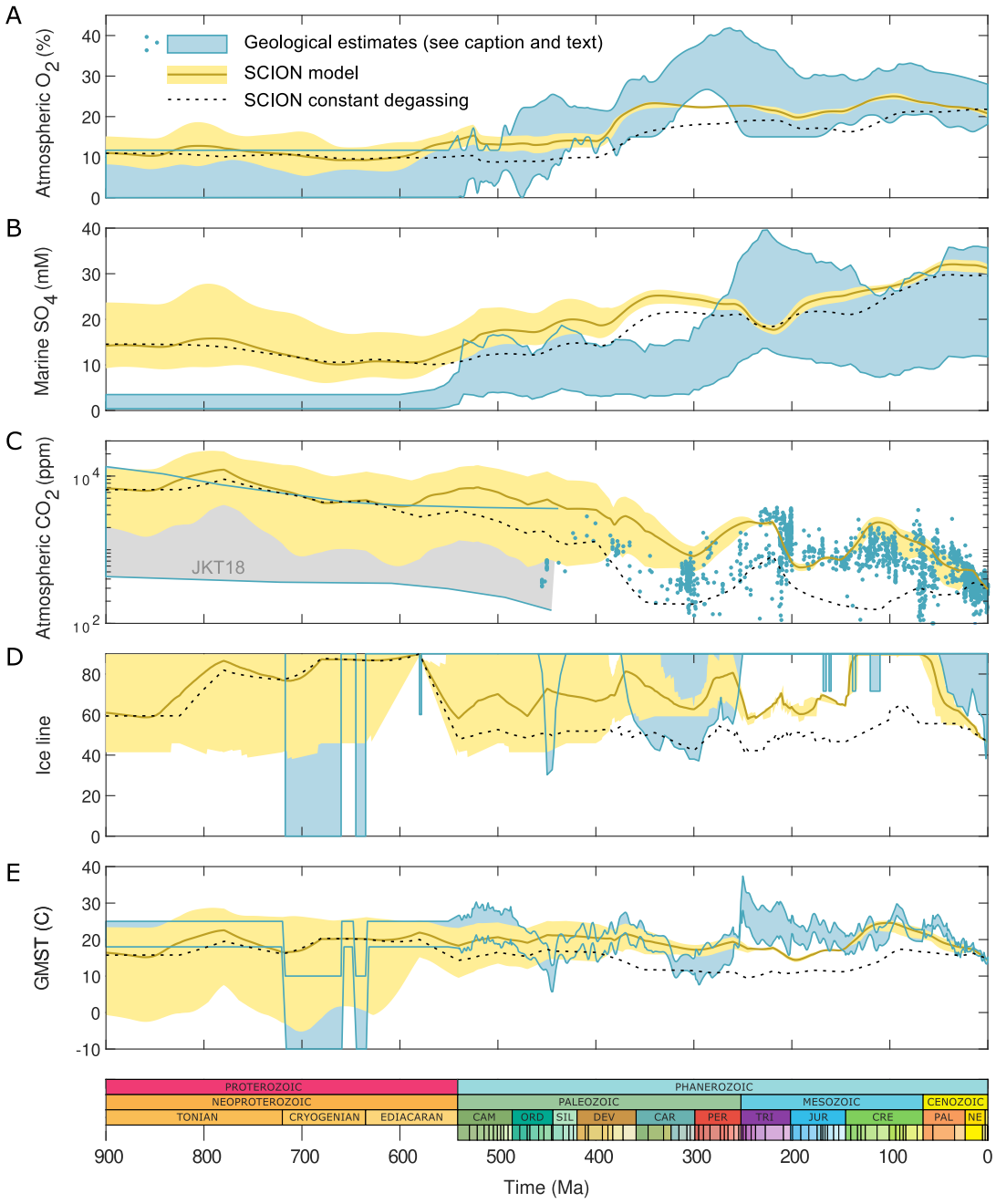

Fig. 3. Key model time-dependent outputs compared to geological estimates. A. Atmospheric oxygen (compared to Mills et al., 2023). B. Marine sulfate (compared to Algeo et al., 2015; Canfield and Farquhar, 2009). C. Atmospheric carbon dioxide (compared to Foster et al., 2017; Witkowski et al., 2018; and the model of Krissansen-Totton et al., 2018 (JKT18) for the Precambrian). D. Ice line latitude – extent of ice caps (compared to Scotese, 2021). E. Global Mean Surface Temperature (GMST, compared to Scotese et al., 2021 for the Phanerozoic, with the Cambrian greenhouse temperature range extended into the Neoproterozoic except for during the Snowball Earth glaciations). Model ensemble range is shown in yellow with the centre line showing the mean estimates. The grey dashed line shows the mean from an alternative model simulation, which assumes a fixed present day degassing rate for the whole run.

included processes like degassing rates.

As with previous SCION simulations for the Paleozoic (Mills et al., 2021), Neoproterozoic sulfate levels in SCION are higher than those inferred from the geological record (which is largely based on the observed isotopic fractionation between sulfate and pyrite and the proposed lack of gypsum deposition; Canfield and Farquhar, 2009). Recent work (Krause et al., 2024) concluded that overestimation of Paleozoic sulfate levels in biogeochemical box models was primarily driven by a poor representation of the calcium cycle in these models. We therefore speculate that adding a dynamic calcium cycle to SCION would improve the model-data mismatch here. Lower modelled oxygen levels would also reduce pyrite weathering and associated sulfate inputs, likely lowering marine sulfate concentrations further. Outputs of evaporite gypsum may also be related to basin restriction, but although the SCION model uses a loose approximation of this for the Phanerozoic based on coastline length, further variation in this process is not explored for the Neoproterozoic due to high uncertainty in coastlines.

3.2. *Drivers of Neoproterozoic climate and biogeochemistry*

Our work set out to test to what degree changes to paleogeography and degassing rates impacted Neoproterozoic surface conditions. For the

degassing rate, the impact is large, and within the large uncertainty on this forcing we can produce icehouse or greenhouse climates on par with the hottest and coldest stages of the Phanerozoic. We see a mean ~ 6 °C of global cooling moving from the Tonian to the Cryogenian in our model, driven partly by the assumed reduction in degassing rates between these periods. A reduction in ridge generation rate, based on the same underlying tectonic framework, has recently been proposed to have driven the Sturtian Snowball Earth initiation (Dutkiewicz et al., 2024). Our work supports this as a possibility, but more work is clearly needed to reduce the uncertainty in overall tectonic CO_2 degassing rates, which are a function of different plate boundaries and processes (e.g. Müller et al., 2022).

We see a moderate effect from paleogeographic weathering enhancement in our simulations. The paleogeographic model used for the FOAM simulations has a clear transition from an amalgamated Rodinia supercontinent in the Tonian, to largely dispersed continents in the Cryogenian (Fig. 4), but this does not translate to a dramatic change in the overall availability of surface runoff in the way that earlier simpler models had shown (Donnadieu et al., 2004). The dashed line in Fig. 3 shows an alternative model ensemble mean where the degassing rate remains constant at the present-day value for the whole run, to better view the paleogeographic effect on the model. This model output retains the general trend of mid-Tonian warming and subsequent cooling into the Cryogenian, but the overall temperature change is around 3 °C. Thus, the overall effect of degassing and paleogeography on driving Tonian–Cryogenian cooling appears roughly equal in this model, and both act to drive cooling into the Cryogenian. Nevertheless, as above, we do not recreate a major ice sheet expansion and deep cooling event in the Cryogenian because we do not take into account the formation of continental ice sheets (i.e. the ice/snow albedo feedback), and we also do not consider the weathering of continental flood basalts at this time which could reduce temperature further, although these effects are uncertain and would depend on the location of LIPs (Donnadieu et al., 2004; Black et al., 2024). Furthermore, the model also predicts a cool early Tonian, so the broad transition from greenhouse to icehouse during the Neoproterozoic is not clearly reproduced in the model.

3.3. Neoproterozoic isotopic records

The model carbon isotope record (Fig. 5) is stable at about the mean value of the geological record but does not produce any of the well-documented large excursions. Even more so than atmospheric oxygen,

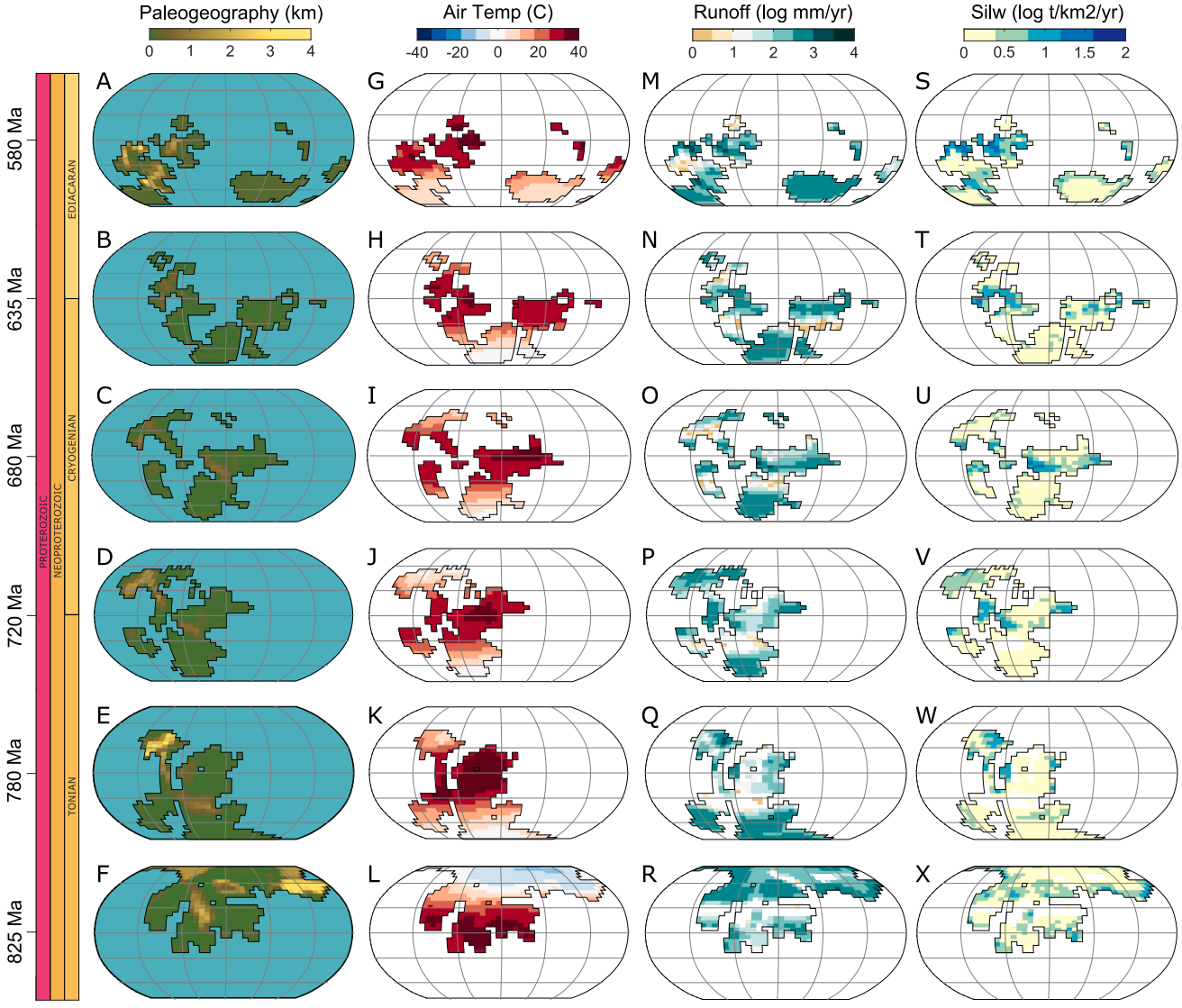

Fig. 4. Model 2D snapshots at keyframe timepoints. A-F. Paleogeography used in the FOAM climate model to produce runs for the emulator in SCION. G-L. SCION model surface air temperature. M-R. SCION model global runoff. S-X. SCION model silicate weathering rate. Note that SCION emulated climate fields are interpolated from GCM runs.

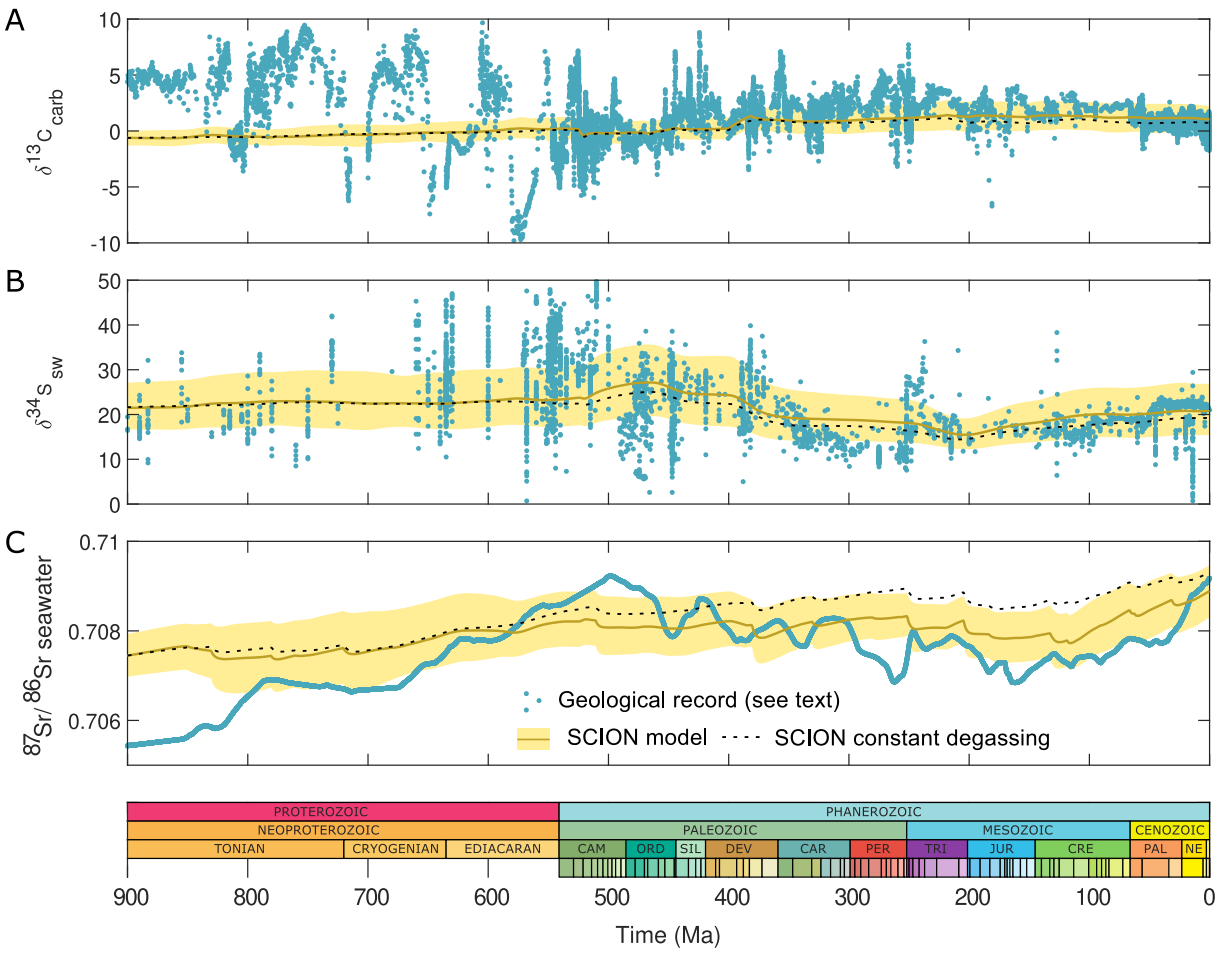

Fig. 5. Model isotope tracers. A. Carbonate carbon isotopes (compared to Cramer and Jarvis, 2020). B. Oceanic sulfur isotopes (compared to Crockford et al., 2019). C. Ocean strontium isotopes (compared to McArthur et al., 2020). Model ensemble range is shown in yellow with the centre line showing the mean estimates. The grey dashed line shows the mean from an alternative model simulation, which assumes a fixed present day degassing rate for the whole run.

the carbon isotope record is likely to respond greatly to events like Snowball Earth and rising marine oxygen levels, which would dramatically alter productivity and remineralization (Hoffman and Schrag, 2002; Rothman et al., 2003). The geological sulfur isotope record has a coarser time resolution, although individual carbon isotope events like the Shuram negative excursion, and subsequent late Ediacaran to early Cambrian positive excursions, do appear to have synchronous excursions in $\delta^{34}S$ (Osburn et al., 2015; Tostevin et al., 2017; He et al., 2019). As with the carbon isotopes, the model can capture the general long-term trend in sulfate sulfur isotopes, but not the individual excursions. Again, this may be because the model does not capture major climatic events throughout this period. Also, these excursions are typically over a shorter timeframe than the variations in the forcings applied to the model, which typically vary significantly only over periods of ~10 Myrs or more. In other words, these excursions are likely not directly caused by long-term tectonic and degassing processes, but by processes with shorter characteristic timescales, such as those associated with the organic carbon cycle.

The model strontium isotope record rises between the Cryogenian and Cambrian due to our assumption that the global area of granitic lithologies rises over this time, and due to radioactive decay, which drives a slow but continuous rise in strontium isotopes over time. More detailed work using the same climate simulations, but which also uses spatial maps of radiogenic and unradiogenic crust (i.e. continental shield, arcs and LIPs) also predicts a rise in $^{87}Sr/^{86}Sr$ over this time, and to a greater degree, due primarily to weathering of radiogenic crust during the Pan-African orogens (Goddéris et al., 2017a, 2017b).

3.4. Sensitivity to long-term forcings

In Fig. 6 we explore the model sensitivity to changing the values of the basalt area, granite area and degassing rate by fixing these at different assumed static values throughout the model run, while allowing all the other model parameters to vary as normal. The exposed granite and basalt area forcings (Fig. 6a,b) influence only the model strontium isotope ratios, as differential reactivities of these lithologies are not included. Predictably therefore, higher granite areas cause the model $^{87}Sr/^{86}Sr$ ratio to rise, and higher basalt areas cause it to fall. Much of the Phanerozoic strontium isotope record can be explained by basalt and granite area variations within this framework, although this analysis ignores the geographic location of these lithologies, which is very important for their weathering fluxes. Instead, when varying the model degassing rate (Fig. 6c), large variations in the $^{87}Sr/^{86}Sr$ record, that broadly encompass the proxy range, can be achieved. Overall, known processes seem potentially capable of driving the $^{87}Sr/^{86}Sr$ variations seen in the geological record, although reproducing the very low values in the early Tonian would require a combination of very high degassing rates, high basaltic areas and low granitic areas. In Fig. 6d, we explore the effects of modifying the model degassing rate, on the predicted global mean surface temperature. The geological temperature reconstruction shown is broadly reproducible in the model with degassing rates ranging from 50 % to 400 % of present-day rates. Outliers here are the early Triassic, where additional carbon was added from the Siberian Traps LIP (Svensen et al., 2009), and the Cryogenian glaciations, where ice albedo effects not included in the model likely drove

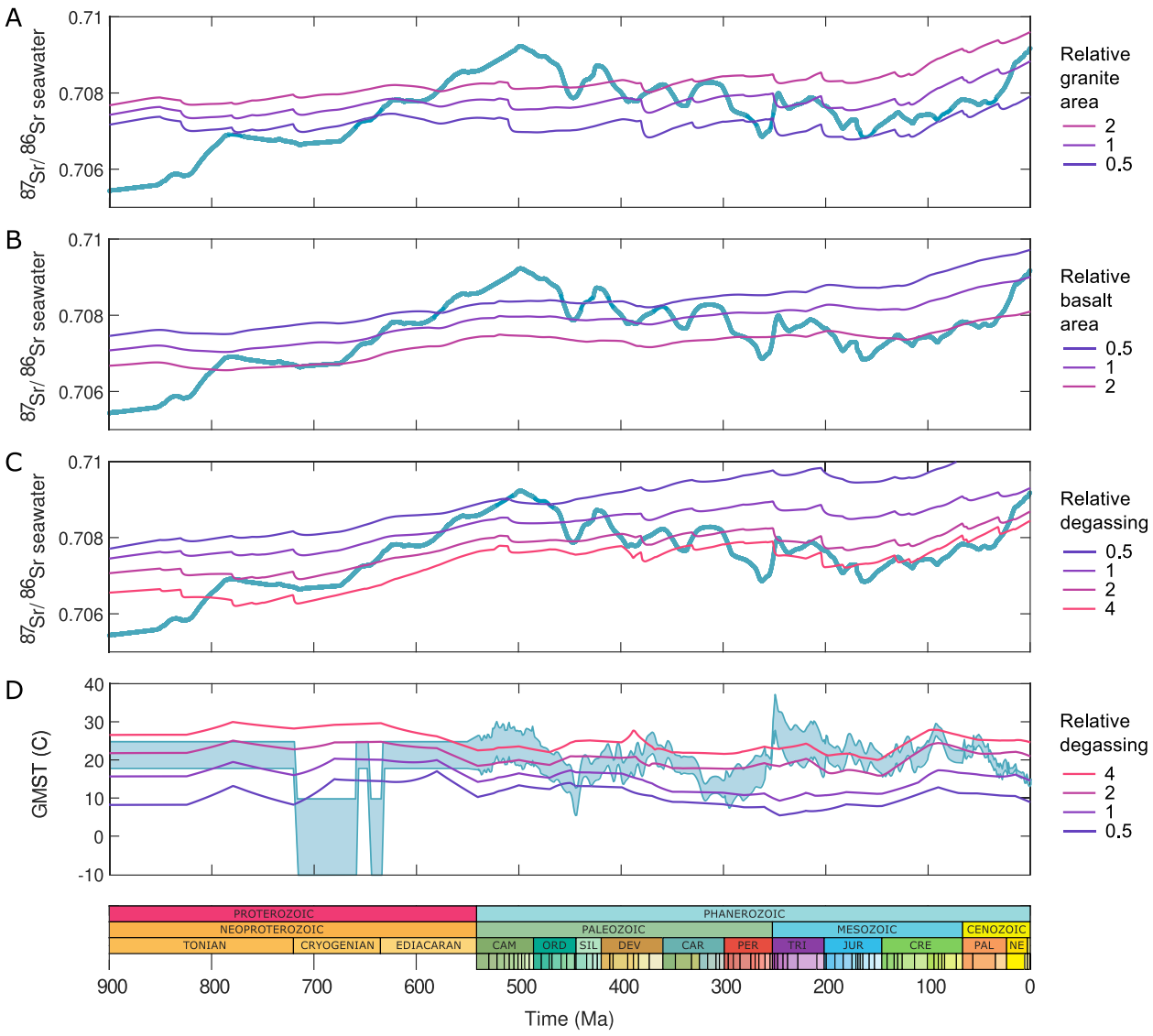

Fig. 6. Fixed forcing model runs. A-C. Model seawater strontium isotope ratios for fixed forcing runs where a single forcing (A – granite area; B – basalt area; C – degassing rate) is fixed at the given value for the whole model run. D. Model Global Mean Surface Temperature for fixed degassing rate runs.

extremely low temperatures (Hoffman et al., 2017). Very high sustained global temperatures above 30 °C, as have been proposed for several hothouse periods (e.g. Grossman and Joachimski, 2022; Judd et al., 2024), would require degassing rates above 400 % of the present day in SCION (similar to conclusions based on the GEOCLIM model – Marcilly et al., 2022).

4. Conclusions and future work

Our extension of SCION into the Neoproterozoic produces a long-term baseline estimate for atmospheric O_2, CO_2 and global average surface temperature that is reasonably in line with the long-term geological record. We show that, according to the available continental distribution, climate model ensemble and tectonic degassing rate reconstructions, our model predicts that combined paleogeographic weathering enhancement and a reduction in CO_2 degassing could have driven ~6 °C of global cooling between the mid-late Tonian and Cryogenian. However, the uncertainty range on these results is very large, and the model also predicts a cool early Tonian, which is not clearly supported by the geological record. Furthermore, our model does not produce the dramatic climate and biogeochemical changes that are expected during the initiation and termination of Snowball Earth glaciations, and the large isotope excursions that are broadly associated with these. This is most likely because we have only considered the long-term tectonic setting (e.g. degassing, paleogeographies) to reconstruct the Earth's deep time climate. However, even a longer-term descent into a Snowball Earth glaciation could not convincingly occur in the model because it does not consider variable continental ice sheets. The SCION model also has a low climate sensitivity, which is set by the climate sensitivity of the FOAM climate model used to produce the emulator, and may drive overestimation of atmospheric CO_2 levels (Mills et al., 2021). The long-term 'Earth System Sensitivity' to a doubling of CO_2 is about 3 °C in SCION, as opposed to the 5–8 °C suggested by some proxy compilations (e.g. Hönisch et al., 2023; Judd et al., 2024). Thus, larger variations in modelled temperature and surface conditions may also be possible if a climate model with higher CO_2-sensitivity were used to build the emulator.

Large swings in carbon isotope ratios in the Neoproterozoic geological record underscore the premise that large changes to production and remineralization processes may have occurred during these periods, which are not modelled here. These excursions may also be related to the evolution of novel planktonic cyanobacteria (i.e. *Trichodesmium, Crocosphaera, Synechococcus, Prochlorococcus*; Sánchez-Baracaldo et al., 2014, Sánchez-Baracaldo, 2015, Boden et al., 2021; Fournier et al.,

2021) and the rise of algae to ecological dominance (Brocks et al., 2017, 2023). The Neoproterozoic saw the ecological expansion of both planktonic cyanobacteria (Sánchez-Baracaldo et al., 2014; Sánchez-Baracaldo, 2015; Fournier et al., 2021) and green algae (Brocks et al., 2017; Del Cortona et al., 2020; Sanchez-Baracaldo et al., 2017), and it has been proposed that the emergence of these novel primary producers could have increased the strength of the marine biological pump, contributing to the Neoproterozoic collapse of widespread euxinia and dominance of oxygenic photosynthesis in the ocean (Sánchez-Baracaldo et al., 2014). Remineralisation processes may also have changed fundamentally, including and the potential oxidation of dissolved organic carbon in the ocean during periods of ventilation (e.g. the Shuram excursion; Rothman et al., 2003). It has been shown in the COPSE model – which models the ocean in the same way as SCION – that large excursions in Ediacaran seawater $\delta^{13}C$ and $\delta^{34}S$ values could be driven by the input of sulfate from weathering and subsequent oxidation of marine dissolved organic carbon (Shields et al., 2019). It has also been shown in COPSE that prolonged periods of high global temperatures and elevated weathering following Snowball Earth deglaciation could drive large and protracted positive excursions in seawater $\delta^{13}C$ (Mills et al., 2011). These ideas can be more fully tested in future versions of SCION that build on the baseline presented here. Finally, our model also overestimates Precambrian marine sulfate concentrations considerably, which perhaps may be resolved by consideration of a dynamic calcium reservoir in future model versions (Krause et al., 2024).

Nevertheless, we believe that this model provides a useful baseline for further investigation of the drivers of Neoproterozoic climate and biogeochemical change. We suggest that the following processes or mechanisms should be added to the model—or others of this type—to better understand these:

- Dynamic continental lithology, including the Franklin LIP and continental arcs. These areas should produce additional silicate weathering fluxes, and variable Sr isotope ratios (e.g. Park et al., 2021).
- Dynamic continental ice sheets. These are essential for simulating the degree of cooling during Snowball Earth glaciations (e.g. Hoffman et al., 2017). This could be achieved by coupling an ice sheet model (parameterised or full 3D thermomechanical representation) with the GCM to incorporate ice sheet-climate positive feedbacks (i.e. ice-albedo and orography-lapse rate) and other climate responses associated with ice sheet inception and growth.
- Evolution of primary producers and their ecological expansion. Changing relationships between productivity and nutrients, the efficiency of the biological pump, and the depth of remineralization, may impact the carbon cycle considerably (e.g. Lenton et al., 2014).
- Calcium cycling. Large mismatches in sulfate concentrations may be driving additional mismatches (e.g. through over-abundance of oxidants), and this may be solved by including a dynamic calcium cycle (Krause et al., 2024).

It is likely that these additions would also improve the model's ability to reproduce Phanerozoic climate and biogeochemistry. However, for both the Neoproterozoic and Phanerozoic, further work to better constrain paleogeography (including topography and bathymetry) and degassing rates are also essential. Degassing is a first-order driver of CO_2 levels and climate, while different paleogeographic reconstructions (e.g. Torsvik and Cocks, 2017) may place important landmasses inside or outside of warm and wet climate zones, which could make significant differences to global silicate weathering. Differences in heights and locations of mountains, and in seafloor bathymetry, may also change global climate in ways that are difficult to predict. The positioning of coastlines and overall area of flooded versus exposed continents is also important in setting global weathering rates and is extremely uncertain for the Neoproterozoic. Building climate emulators with alternative paleogeographies and underlying physical climate models is essential, but is an extremely time-consuming process. Indeed, the emulator constructed here would benefit from higher time-resolution. Paleogeographic features may change substantially between the current climate model timepoint separation of around 50 Myrs in ways that cannot be well-approximated by even advanced neural network interpolation methods, and physical climate simulations should ideally be made on resolutions of around 20 Myrs or less (Zheng et al., 2024). Finally, it is important to build better time-constrained series of geological and geochemical indicators for the Neoproterozoic and especially the Tonian period. The apparent lack of variability in climate, atmospheric oxygen and marine sulfate proxies here is largely due to a lack of data.

Code access

Model code for SCION version 1.2.0 including full documentation and derivation can be accessed at https://github.com/bjwmills/SCION

Tutorials on running the SCION model can be accessed at: https://earthevolutionmodelling.com/code

Rights

CRediT authorship contribution statement

Benjamin J.W. Mills: Writing – review & editing, Writing – original draft, Visualization, Validation, Software, Resources, Project administration, Methodology, Investigation, Funding acquisition, Formal analysis, Data curation, Conceptualization. **Guillaume le Hir:** Writing – review & editing, Validation, Software, Resources, Investigation, Formal analysis, Data curation, Conceptualization. **Andrew Merdith:** Writing – review & editing, Validation, Software, Resources, Investigation, Formal analysis, Data curation. **Khushboo Gurung:** Writing – review & editing, Validation, Investigation, Formal analysis. **Fred T. Bowyer:** Writing – review & editing, Validation, Investigation, Formal analysis. **Alexander J. Krause:** Writing – review & editing, Validation, Investigation, Formal analysis. **Patricia Sanchez-Baracaldo:** Writing – review & editing, Validation, Investigation, Formal analysis. **Stephen J. Hunter:** Writing – review & editing, Visualization, Investigation, Formal analysis. **Yinggang Zhang:** Writing – review & editing, Validation, Investigation, Formal analysis.

Declaration of competing interest

The authors declare that they have no known competing financial interests or personal relationships that could have appeared to influence the work reported in this paper.

Acknowledgements

BJWM and ASM acknowledge UKRI grant NE/X011208/1 and EU MSCA-IF project 893615. BJWM, KG, FTB, AJK and SJH acknowledge UKRI grant EP/Y008790/1. YZ acknowledges the China Postdoctoral Science Foundation project 2023M733592. ASM acknowledges ARC DECRA Fellowship DE230101642. Funding support for this work came from a Royal Society University Research Fellowship to PSB.

Data availability

All code and data included in supplement and will be made free online if published

References

Alcott, L.J., Walton, C., Planavsky, N.J., Shorttle, O., Mills, B.J.W., 2024. Crustal carbonate build-up as a driver for Earth's oxygenation. Nat. Geosci. 17, 458–464. https://doi.org/10.1038/s41561-024-01417-1.

Algeo, T.J., Ingall, E., 2007. Sedimentary Corg:P ratios, paleocean ventilation, and Phanerozoic atmospheric pO2. Paleogeogr. Paleoclimatol. Paleoecol. 256, 130–155.

Algeo, T.J., Luo, G.M., Song, H.Y., Lyons, T.W., Canfield, D.E., 2015. Reconstruction of secular variation in seawater sulfate concentrations. Biogeosciences 12, 2131–2151. https://doi.org/10.5194/bg-12-2131-2015.

Arvidson, R.S., Mackenzie, F.T., Guidry, M.W., 2013. Geologic history of seawater: a MAGic approach to carbon chemistry and ocean ventilation. Chem. Geol. 362, 287–304. https://doi.org/10.1016/j.chemgeo.2013.10.012.

Bergman, Noam M., Lenton, Timothy M., Watson, Andrew J., 2004. COPSE: a new model of biogeochemical cycling over Phanerozoic time. Am. J. Sci. 304, 397–437.

Berner, Robert A., 1991. A model for atmospheric CO2 over Phanerozoic time. Am. J. Sci. 291, 339–376.

Berner, Robert A., 1997. The rise of Plants and their effect on Weathering and Atmospheric CO2. Science 276, 544–546.

Berner, Robert A., 2006. GEOCARBSULF: a combined model for Phanerozoic atmospheric O2 and CO2. Geochim. Cosmochim. Acta 70, 5653–5664.

Berner, Robert A., 2009. Phanerozoic atmospheric oxygen: new results using the GEOCARBSULF model. Am. J. Sci. 309, 603–606.

Berner, Robert A., Canfield, Donald E., 1989. A new model for atmospheric oxygen over Phanerozoic time. Am. J. Sci. 289, 333–361.

Black, B.A., et al., 2024. Cryptic degassing and protracted greenhouse climates after flood basalt events. Nat. Geosci. 1–7. https://doi.org/10.1038/s41561-024-01574-3.

Bluth, Gregg J.S., Kump, Lee R., 1991. Phanerozoic Paleogeology. Am. J. Sci. 291, 284–308.

Boden, J.S., Konhauser, K.O., Robbins, L.J., Sánchez-Baracaldo, P., 2021. Timing the evolution of antioxidant enzymes in cyanobacteria. Nat. Commun. 12, 4742. https://doi.org/10.1038/s41467-021-24396-y.

Brocks, J.J., Jarrett, A.J.M., Sirantoine, E., Hallmann, C., Hoshino, Y., Liyanage, T., 2017. The rise of algae in Cryogenian oceans and the emergence of animals. Nature 548, 578–581. https://doi.org/10.1038/nature23457.

Brocks, J.J., Nettersheim, B.J., Adam, P., Schaeffer, P., Jarrett, A.J.M., Guneli, N., Liyanage, T., van Maldegem, L.M., Hallmann, C., Hope, J.M., 2023. Lost world of complex life and the late rise of the eukaryotic crown. Nature 618 (7966), 767–773.

Brune, S., Williams, S.E., Müller, R.D., 2017. Potential links between continental rifting, CO2 degassing and climate change through time. Nat. Geosci. 10, 941–946. https://doi.org/10.1038/s41561-017-0003-6.

Canfield, D.E., 1998. A new model for Proterozoic Ocean chemistry. Nature 396, 450–453.

Canfield, D.E., Farquhar, J., 2009. Animal evolution, bioturbation, and the sulfate concentration of the oceans. Proc. Natl. Acad. Sci. USA 106, 8123–8127. https://doi.org/10.1073/pnas.0902037106.

Canfield, Don E., Poulton, Simon W., Narbonne, Guy M., 2007. Late-Neoproterozoic Deep-Ocean Oxygenation and the rise of Animal Life. Science 315, 92–95.

Cramer, B.D., Jarvis, I., 2020. Chapter 11 - Carbon Isotope Stratigraphy. In: Gradstein, F. M., Ogg, J.G., Schmitz, M.D., Ogg, G.M. (Eds.), Geologic Time Scale 2020. Elsevier, pp. 309–343. https://doi.org/10.1016/B978-0-12-824360-2.00011-5.

Crockford, P.W., et al., 2019. Claypool continued: Extending the isotopic record of sedimentary sulfate. Chem. Geol. 513, 200–225.

Dahl, Tais W., Hammarlund, Emma U., Anbar, Ariel D., Bond, David P.G., Gill, Benjamin C., Gordon, Gwyneth W., Knoll, Andrew H., Nielsen, Arne T., Schovsbo, Niels H., Canfield, Donald E., 2010. Devonian rise in atmospheric oxygen correlated to the radiations of terrestrial plants and large predatory fish. PNAS 107, 17911–17915.

Del Cortona, A., Jackson, C.J., Bucchini, F., Van Bel, M., D'Hondt, S., Skaloud, P., Delwiche, C.F., Knoll, A.H., Raven, J.A., Verbruggen, H., et al., 2020. Neoproterozoic origin and multiple transitions to macroscopic growth in green seaweeds. Proc. Natl. Acad. Sci. USA 117 (5), 2551–2559.

Domeier, M., Torsvik, T.H., 2017. Full-plate modelling in pre-Jurassic time. Geol. Mag. 156, 261–280. https://doi.org/10.1017/s0016756817001005.

Domeier, M., Magni, V., Hounslow, M.W., Torsvik, T.H., 2018. Episodic zircon age spectra mimic fluctuations in subduction. Sci. Rep. 8, 17471.

Donnadieu, Y., Godderis, Y., Ramstein, G., Nedelec, A., Meert, J., 2004. A "snowball Earth" climate triggered by continental break-up through changes in runoff. Nature 428, 303–306. https://doi.org/10.1038/nature02408.

Dunn, F.S., Kenchington, C.G., Parry, L.A., Clark, J.W., Kendall, R.S., Wilby, P.R., 2022. A crown-group cnidarian from the Ediacaran of Charnwood Forest, UK. Nat. Ecol. Evolut. 6, 1095–1104.

Dutkiewicz, A., Merdith, A.S., Collins, A.S., Mather, B., Ilano, L., Zahirovic, S., Müller, R. D., 2024. Duration of Sturtian "Snowball Earth" glaciation linked to exceptionally low mid-ocean ridge outgassing. Geology 52, 292–296. https://doi.org/10.1130/G51669.1.

Ernst, R.E., Youbi, N., 2017. How large Igneous Provinces affect global climate, sometimes cause mass extinctions, and represent natural markers in the geological record. Palaeogeogr. Palaeoclimatol. Palaeoecol. 478, 30–52. https://doi.org/10.1016/j.palaeo.2017.03.014.

Foster, G.L., Royer, D.L., Lunt, D.J., 2017. Future climate forcing potentially without precedent in the last 420 million years. Nat. Commun. 8, 14845.

Fournier, G.P., Moore, K.R., Rangel, L.T., Payette, J.G., Momper, L., Bosak, T., 2021. The Archean origin of oxygenic photosynthesis and extant cyanobacterial lineages. Proceed. Royal Soc. B-Biol. Sci. 288 (1959).

Goddéris, Y., Donnadieu, Y., Le Hir, G., Lefebvre, V., Nardin, E., 2014. The role of palaeogeography in the Phanerozoic history of atmospheric CO2 and climate. Earth Sci. Rev. 128, 122–138. https://doi.org/10.1016/j.earscirev.2013.11.004.

Goddéris, Y., Donnadieu, Y., Carretier, S., Aretz, M., Dera, G., Macouin, M., Regard, V., 2017a. Onset and ending of the late Palaeozoic ice age triggered by tectonically paced rock weathering. Nat. Geosci. 10, 382–386. https://doi.org/10.1038/ngeo2931.

Goddéris, Y., Le Hir, G., Macouin, M., Donnadieu, Y., Hubert-Théou, L., Dera, G., Aretz, M., Fluteau, F., Li, Z.X., Halverson, G.P., 2017b. Paleogeographic forcing of the strontium isotopic cycle in the Neoproterozoic. Gondwana Res. 42, 151–162. https://doi.org/10.1016/j.gr.2016.09.013.

Goddéris, Y., Donnadieu, Y., Mills, B.J.W., 2023. What Models tell Us about the Evolution of Carbon sources and Sinks over the Phanerozoic. Annu. Rev. Earth Planet. Sci. 51, 471–492. https://doi.org/10.1146/annurev-earth-032320-092701.

Grossman, E.L., Joachimski, M.M., 2022. Ocean temperatures through the Phanerozoic reassessed. Sci. Rep. 12, 8938.

Gurung, K., Field, K.J., Batterman, S.A., Godderis, Y., Donnadieu, Y., Porada, P., Taylor, L.L., Mills, B.J.W., 2022. Climate windows of opportunity for plant expansion during the Phanerozoic. Nat. Commun. 13, 4530. https://doi.org/10.1038/s41467-022-32077-7.

Gurung, K., Field, K.J., Batterman, S.A., Poulton, S.W., Mills, B.J.W., 2024. Geographic range of plants drives long-term climate change. Nat. Commun. 15, 1805. https://doi.org/10.1038/s41467-024-46105-1.

He, T., Zhu, M., Mills, B.J.W., Wynn, P.M., Zhuravlev, A.Yu., Tostevin, R., Pogge von Strandmann, P.A.E., Yang, A., Poulton, S.W., Shields, G.A., 2019. Possible links between extreme oxygen perturbations and the Cambrian radiation of animals. Nat. Geosci. 12, 468–474.

Hoffman, Paul F., Kaufman, Alan J., Halverson, Galen P., Schrag, Daniel P., 1998. A Neoproterozoic Snowball Earth. Science 281, 1342–1346.

Hoffman, P.F., Abbot, D.S., Ashkenazy, Y., Benn, D.I., Brocks, J.J., Cohen, P.A., Cox, G. M., Creveling, J.R., Donnadieu, Y., Erwin, D.H., Fairchild, I.J., Ferreira, D., Goodman, J.C., Halverson, G.P., Jansen, M.F., Le Hir, G., Love, G.D., Macdonald, F. A., Maloof, A.C., Partin, C.A., Ramstein, G., Rose, B.E.J., Rose, C.V., Sadler, P.M., Tziperman, E., Voigt, A., Warren, S.G., 2017. Snowball Earth climate dynamics and Cryogenian geology-geobiology. Sci. Adv. 3, e1600983. https://doi.org/10.1126/sciadv.1600983.

Hoffman, Paul F., Schrag, Daniel P., 2002. The snowball Earth hypothesis: testing the limits of global change. Terra Nova 14, 129–155.

Hönisch, B., Royer, D.L., Breecker, D.O., Polissar, P.J., Bowen, G.J., Henehan, M.J., Cui, Y., Steinthorsdottir, M., McElwain, J.C., Kohn, M.J., Pearson, A., Phelps, S.R., Uno, K.T., Ridgwell, A., Anagnostou, E., Austermann, J., Badger, M.P.S., Barclay, R. S., Bijl, P.K., Chalk, T.B., Scotese, C.R., de la Vega, E., DeConto, R.M., Dyez, K.A., Ferrini, V., Franks, P.J., Giulivi, C.F., Gutjahr, M., Harper, D.T., Haynes, L.L., Huber, M., Snell, K.E., Keisling, B.A., Konrad, W., Lowenstein, T.K., Malinverno, A., Guillermic, M., Mejía, L.M., Milligan, J.N., Morton, J.J., Nordt, L., Whiteford, R., Roth-Nebelsick, A., Rugenstein, J.K.C., Schaller, M.F., Sheldon, N.D., Sosdian, S., Wilkes, E.B., Witkowski, C.R., Zhang, Y.G., Anderson, L., Beerling, D.J., Bolton, C., Cerling, T.E., Cotton, J.M., Da, J., Ekart, D.D., Foster, G.L., Greenwood, D.R., Hyland, E.G., Jagniecki, E.A., Jasper, J.P., Kowalczyk, J.B., Kunzmann, L., Kürschner, W.M., Lawrence, C.E., Lear, C.H., Martínez-Botí, M.A., Maxbauer, D.P., Montagna, P., Naafs, B.D.A., Rae, J.W.B., Raitzsch, M., Retallack, G.J., Ring, S.J., Seki, O., Sepúlveda, J., Sinha, A., Tesfamichael, T.F., Tripati, A., van der Burgh, J., Yu, J., Zachos, J.C., Zhang, L., 2023. Cenozoic CO2 Proxy Integration Project (CenCO2PIP) Consortium, Toward a Cenozoic history of atmospheric CO2. Science 382, eadi5177.

Jacob, R., 1997. Low Frequency Variability in a Simulated Atmosphere Ocean System. Ph.D. thesis. University of Wisconsin-Madison.

Judd, E.J., et al., 2024. A 485-million-year history of Earth's surface temperature. Science 385, eadk3705.

Krause, A.J., Mills, B.J.W., Zhang, S., Planavsky, N.J., Lenton, T.M., Poulton, S.W., 2018. Stepwise oxygenation of the Paleozoic atmosphere. Nat. Commun. 9, 4081. https://doi.org/10.1038/s41467-018-06383-y.

Krause, Alexander J., Mills, Benjamin J.W., Merdith, Andrew S., Lenton, Timothy M., Poulton, Simon W., 2022. Extreme variability inatmospheric oxygen levels in the late Precambrian. Sci. Adv. 8, eabm8191.

Krause, A.J., Shields, G.A., Newton, R.J., Mills, B.J.W., 2024. Modelling sulfate concentrations in the global ocean through Phanerozoic time. JGS 181 jgs2023-184.

Krissansen-Totton, J., Arney, G.N., Catling, D.C., 2018. Constraining the climate and ocean pH of the early Earth with a geological carbon cycle model. Proc. Natl. Acad. Sci. USA 115, 4105–4110.

Le Hir, G., Teitler, Y., Fluteau, F., Donnadieu, Y., Philippot, P., 2014. The faint young Sun problem revisited with a 3-D climate–carbon model – part 1. Clim. Past 10, 697–713.

Lenton, Timothy M., 2001. The role of land plants, phosphorus weathering and fire in the rise and regulation of atmospheric oxygen. Glob. Chang. Biol. 7, 613–629.

Lenton, Timothy M., Crouch, Michael, Johnson, Martin, Pires, Nuno, Dolan, Liam, 2012. First plants cooled the Ordovician. Nat. Geosci. 5, 86–89.

Lenton, Timothy M., Boyle, Richard A., Poulton, Simon W., Shields-Zhou, Graham A., Butterfield, Nicholas J., 2014. Co-evolution of eukaryotes and ocean oxygenation in the Neoproterozoic Era. Nat. Geosci. https://doi.org/10.1038/ngeo2108.

Lenton, T.M., Dahl, T.W., Daines, S.J., Mills, B.J., Ozaki, K., Saltzman, M.R., Porada, P., 2016. Earliest land plants created modern levels of atmospheric oxygen. Proc. Natl. Acad. Sci. USA 113, 9704–9709. https://doi.org/10.1073/pnas.1604787113.

Lenton, T.M., Daines, S.J., Mills, B.J.W., 2018. COPSE reloaded: An improved model of biogeochemical cycling over Phanerozoic time. Earth Sci. Rev. 178, 1–28. https://doi.org/10.1016/j.earscirev.2017.12.004.

Li, Z.-X., Evans, D.A.D., Halverson, G.P., 2013. Neoproterozoic glaciations in a revised global palaeogeography from the breakup of Rodinia to the assembly of Gondwanaland. Sediment. Geol. 294, 219–232. https://doi.org/10.1016/j.sedgeo.2013.05.016.

Longman, J., Mills, B.J.W., Manners, H.R., Gernon, T.M., Palmer, M.R., 2021. Late Ordovician climate change and extinctions driven by elevated volcanic nutrient supply. Nat. Geosci. 14, 924–929. https://doi.org/10.1038/s41561-021-00855-5.

Maffre, P., Ladant, J.-B., Moquet, J.-S., Carretier, S., Labat, D., Goddéris, Y., 2018. Mountain ranges, climate and weathering. Do orogens strengthen or weaken the silicate weathering carbon sink? Earth Planet. Sci. Lett. 493, 174–185. https://doi.org/10.1016/j.epsl.2018.04.034.

Maher, K., Chamberlain, C.P., 2014. Hydrologic regulation of chemical weathering and the geologic carbon cycle. Science 343, 1502–1504. https://doi.org/10.1126/science.1250770.

Marcilly, C.M., Torsvik, T.H., Domeier, M., Royer, D.L., 2021. New paleogeographic and degassing parameters for long-term carbon cycle models. Gondwana Res. 97, 176–203. https://doi.org/10.1016/j.gr.2021.05.016.

Marcilly, C.M., et al., 2022. Understanding the early Paleozoic carbon cycle balance and climate change from modelling. Earth Planet. Sci. Lett. 594.

McArthur, J.M., Howarth, R.J., Shields, G.A., Zhou, Y., 2020. Chapter 7 - Strontium Isotope Stratigraphy. In: Gradstein, F.M., Ogg, J.G., Schmitz, M.D., Ogg, G.M. (Eds.), Geologic Time Scale 2020. Elsevier, pp. 211–238. https://doi.org/10.1016/B978-0-12-824360-2.00007-3.

Merdith, A.S., Williams, S.E., Collins, A.S., Tetley, M.G., Mulder, J.A., Blades, M.L., Young, A., Armistead, S.E., Cannon, J., Zahirovic, S., Müller, R.D., 2021. Extending full-plate tectonic models into deep time: linking the Neoproterozoic and the Phanerozoic. Earth Sci. Rev. 214. https://doi.org/10.1016/j.earscirev.2020.103477.

Mills, B., Watson, Andrew J., Goldblatt, Colin, Boyle, Richard, Lenton, Timothy M., 2011. Timing of Neoproterozoic glaciations linked to transport-limited global weathering. Nat. Geosci. 4, 861–864.

Mills, B., Daines, S.J., Lenton, T.M., 2014. Changing tectonic controls on the long-term carbon cycle from Mesozoic to present. Geochem. Geophys. Geosyst. 15, 4866–4884. https://doi.org/10.1002/2014gc005530.

Mills, B.J.W., Scotese, C.R., Walding, N.G., Shields, G.A., Lenton, T.M., 2017. Elevated CO2 degassing rates prevented the return of Snowball Earth during the Phanerozoic. Nat. Commun. 8, 1110. https://doi.org/10.1038/s41467-017-01456-w.

Mills, B.J.W., Krause, A.J., Scotese, C.R., Hill, D.J., Shields, G.A., Lenton, T.M., 2019. Modelling the long-term carbon cycle, atmospheric CO2, and Earth surface temperature from late Neoproterozoic to present day. Gondwana Res. 67, 172–186. https://doi.org/10.1016/j.gr.2018.12.001.

Mills, B.J.W., Donnadieu, Y., Goddéris, Y., 2021. Spatial continuous integration of Phanerozoic global biogeochemistry and climate. Gondwana Res. 100, 73–86. https://doi.org/10.1016/j.gr.2021.02.011.

Mills, B.J.W., Krause, A.J., Jarvis, I., Cramer, B.D., 2023. Evolution of Atmospheric O2 through the Phanerozoic, Revisited. Annu. Rev. Earth Planet. Sci. 51. https://doi.org/10.1146/annurev-earth-032320-095425.

Müller, R.D., Mather, B., Dutkiewicz, A., Keller, T., Merdith, A., Gonzalez, C.M., Gorczyk, W., Zahirovic, S., 2022. Evolution of Earth's tectonic carbon conveyor belt. Nature 605, 629–639. https://doi.org/10.1038/s41586-022-04420-x.

Osburn, M.R., Owens, J., Bergmann, K.D., Lyons, T.W., Grotzinger, J.P., 2015. Dynamic changes in sulfate sulfur isotopes preceding the Ediacaran Shuram Excursion. Geochim. Cosmochim. Acta 170, 204–224. https://doi.org/10.1016/j.gca.2015.07.039.

Park, Y., Swanson-Hysell, N.L., Lisiecki, L.E., Macdonald, F.A., 2021. Evaluating the Relationship between the Area and Latitude of large Igneous Provinces and Earth's Long-Term climate State. In: Large Igneous Provinces. American Geophysical Union (AGU), pp. 153–168. https://doi.org/10.1002/9781119507444.ch7.

Rothman, Daniel H., Hayes, John M., Summons, Roger E., 2003. Dynamics of the Neoproterozoic carbon cycle. PNAS 100, 8124–8129.

Royer, D.L., Donnadieu, Y., Park, J., Kowalczyk, J., Godderis, Y., 2014. Error analysis of CO2 and O2 estimates from the long-term geochemical model GEOCARBSULF. Am. J. Sci. 314, 1259–1283. https://doi.org/10.2475/09.2014.01.

Sánchez-Baracaldo, P., 2015. Origin of marine planktonic cyanobacteria. Sci. Rep. 5, 17418.

Sánchez-Baracaldo, P., Ridgwell, A., Raven, J.A., 2014. A Neoproterozoic transition in the marine nitrogen cycle. Curr. Biol. 24 (6), 652–657.

Sanchez-Baracaldo, P., Raven, J.A., Pisani, D., Knoll, A.H., 2017. Early photosynthetic eukaryotes inhabited low-salinity habitats. Proc. Natl. Acad. Sci. USA 114 (37), E7737–E7745.

Scotese, C.R., 2021. An Atlas of Phanerozoic Paleogeographic Maps: the Seas come in and the Seas Go out. Annu. Rev. Earth Planet. Sci. 49.

Scotese, C.R., Song, H., Mills, B.J.W., van der Meer, D.G., 2021. Phanerozoic paleotemperatures: the earth's changing climate during the last 540 million years. Earth Sci. Rev. 215.

Shields, G.A., Mills, B.J.W., Zhu, M., Raub, T.D., Daines, S.J., Lenton, T.M., 2019. Unique Neoproterozoic carbon isotope excursions sustained by coupled evaporite dissolution and pyrite burial. Nat. Geosci. 12, 823–827. https://doi.org/10.1038/s41561-019-0434-3.

Song, Huyue, An, Z., Ye, Q., Stüeken, E.E., Li, J., Hu, J., Algeo, T.J., Tian, L., Chu, D., Song, Haijun, Xiao, S., Tong, J., 2023. Mid-latitudinal habitable environment for marine eukaryotes during the waning stage of the Marinoan snowball glaciation. Nat. Commun. 14, 1564. https://doi.org/10.1038/s41467-023-37172-x.

Sperling, E.A., Wolock, C.J., Morgan, A.S., Gill, B.C., Kunzmann, M., Halverson, G.P., Macdonald, F.A., Knoll, A.H., Johnston, D.T., 2015. Statistical analysis of iron geochemical data suggests limited late Proterozoic oxygenation. Nature 523, 451–454. https://doi.org/10.1038/nature14589.

Stockey, R.G., Cole, D.B., Farrell, U.C., Agić, H., Boag, T.H., Brocks, J.J., Canfield, D.E., Cheng, M., Crockford, P.W., Cui, H., Dahl, T.W., Del Mouro, L., Dewing, K., Dornbos, S.Q., Emmings, J.F., Gaines, R.R., Gibson, T.M., Gill, B.C., Gilleaudeau, G. J., Goldberg, K., Guilbaud, R., Halverson, G., Hammarlund, E.U., Hantsoo, K., Henderson, M.A., Henderson, C.M., Hodgskiss, M.S.W., Jarrett, A.J.M., Johnston, D. T., Kabanov, P., Kimmig, J., Knoll, A.H., Kunzmann, M., LeRoy, M.A., Li, C., Loydell, D.K., Macdonald, F.A., Magnall, J.M., Mills, N.T., Och, L.M., O'Connell, B., Pagès, A., Peters, S.E., Porter, S.M., Poulton, S.W., Ritzer, S.R., Rooney, A.D., Schoepfer, S., Smith, E.F., Strauss, J.V., Uhlein, G.J., White, T., Wood, R.A., Woltz, C. R., Yurchenko, I., Planavsky, N.J., Sperling, E.A., 2024. Sustained increases in atmospheric oxygen and marine productivity in the Neoproterozoic and Palaeozoic eras. Nat. Geosci. 17, 667–674. https://doi.org/10.1038/s41561-024-01479-1.

Svensen, H., et al., 2009. Siberian gas venting and the end-Permian environmental crisis. Earth Planet. Sci. Lett. 277, 490–500.

Torsvik, T.H., Cocks, L.R.M., 2017. Earth History and Palaeogeography. Cambridge University Press, Cambridge. https://doi.org/10.1017/9781316225523.

Tostevin, R., Mills, B.J.W., 2020. Reconciling proxy records and models of Earth's oxygenation during the Neoproterozoic and Palaeozoic. Inter. Focus 10, 20190137. https://doi.org/10.1098/rsfs.2019.0137.

Tostevin, R., He, T., Turchyn, A.V., Wood, R.A., Penny, A.M., Bowyer, F., Antler, G., Shields, G.A., 2017. Constraints on the late Ediacaran sulfur cycle from carbonate associated sulfate. Precambrian Res. 290, 113–125.

Van Der Meer, Douwe G., Zeebe, Richard E., van Hinsbergen, Douwe J.J., Sluijs, Appy, Spakman, Wim, Torsvik, Trond H., 2014. Plate tectonic controls on atmospheric CO2 levels since the Triassic. PNAS 111, 4380–4385.

West, A.J., 2012. Thickness of the chemical weathering zone and implications for erosional and climatic drivers of weathering and for carbon-cycle feedbacks. Geology 40, 811–814. https://doi.org/10.1130/g33041.1.

Williams, J.J., Mills, B.J.W., Lenton, T.M., 2019. A tectonically driven Ediacaran oxygenation event. Nat. Commun. 10, 2690. https://doi.org/10.1038/s41467-019-10286-x.

Witkowski, C.R., Weijers, J.W.H., Blais, B., Schouten, S., Sinninghe Damnste, J.S., 2018. Molecular fossils from phytoplankton reveal secular PCO2 trend over the Phanerozoic. Sci. Adv. 4, eaat4556.

Zheng, D., et al., 2024. Using deep learning to integrate paleoclimate and global biogeochemistry over the Phanerozoic Eon. Geosci. Model Dev. 17, 5413–5429.